LANGMUIR

Effect of Solvent on Convectively Driven Silica Particle Assembly: Decoupling Surface Tension, Viscosity, and Evaporation Rate

Lucien Roach,* David Gonzalez-Rodriguez, Jie Gao, Eric Laurichesse, Alexander Castro-Grijalba, Reiko Oda, Véronique Schmitt, Emilie Pouget, Mona Tréguer-Delapierre, and Glenna L. Drisko*

Read Online

ACCESS | Metrics & More | Article Recommendations | Supporting Information

ABSTRACT: The process of convectively self-assembling particles in films suffers from low reproducibility due to its high dependency on particle concentration, as well as a variety of interactions and physical parameters. Inhomogeneities in flow rates and instabilities at the air–liquid interface are mostly responsible for reproducibility issues. These problems are aggravated by adding multiple components to the dispersion, such as binary solvent mixtures or surfactant/polymer additives, both common approaches to control stick-slip behavior. When an additive is used, not only does it change the surface tension, but also the viscosity and the evaporation rate. Worse yet, gradients in these three properties can form, which then lead to Marangoni currents. Here, we use a series of alcohols to study the role of viscosity independently of other solvent properties, to show its impact on stick-slip behavior and interband distances. We show that mixtures of glycerol and alcohol or poly(acrylic acid) and alcohol lead to more complex patterning. Marangoni currents are not always observed in co-solvent systems, being dependent on the rate of solvent evaporation. To produce homogeneous particle assemblies and control stick-slip behavior, gradients must be avoided, and the surface tension and viscosity need both be carefully controlled.
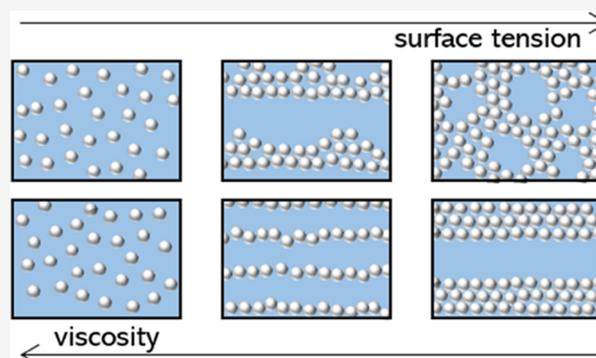
INTRODUCTION

The coffee-ring effect, also referred to as the stick-slip phenomenon, is where particles are brought to the drying line by convective flow and deposited at the edge of a drying front on a substrate. The high concentration of particles pins the meniscus, allowing more particles to come to the contact line, until the meniscus becomes so stretched that it depins, swiftly returning to a resting position. This effect is observed in a drying sessile droplet but also when coupled to directed particle deposition techniques, such as blade-coating and dip-coating. Dip-coating is a simple process, where a substrate is submerged in a particle suspension and then withdrawn at a constant rate. Dip-coating is known to have two dominant regimes based on substrate withdrawal rate; the advective regime or Landau−Levich regime at high withdrawal velocities ($\gtrsim$500 μm s^{-1} for alcohols) and the convective regime at low withdrawal velocities ($\lesssim$500 μm s^{-1} for alcohols). In the advective regime, the particle volume fraction in the meniscus is determined by viscosity, surface tension, and substrate withdrawal rate. In contrast, at slower withdrawal rates, particles are more concentrated in the meniscus relative to the bulk solution via convective flow induced by evaporative flux. Stick-slip banding is common when particle transport is predominately due to convective flow. It is often desirable to control band thickness, interband distance, or even suppress

banding, which is why evaporative particle transport must be understood. Evaporative transport (Q_e) is defined as[1]

$$Q_e \approx c L_c V_e \qquad (1)$$

where c is particle concentration, L_c is capillary length (due to surface tension and substrate wettability), and V_e is evaporation speed (due to solvent volatility, chamber and substrate temperature, and relative humidity, when evaporating water-miscible solvents). To control stick-slip patterning, the easiest solution is often to increase the particle concentration.[2] However, this is not always possible due to particle aggregation at high particle concentrations or difficulties generating large quantities of specialty particles. In these cases, the capillary length can be changed by modifying surface tension,[3] or the hydrophobicity of the substrate can be tuned.[4] Alternatively, V_e can be altered by changing the temperature or dispersant to a solvent with higher volatility. Typically, coatings prepared at temperatures too close to the boiling point lead to
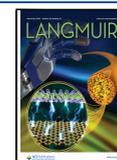
Table 1. Solvent Properties at 50 °C for MeOH, EtOH, *i*-PrOH, and *t*-BuOH

solvent	viscosity[a] (mPa s)	density (g cm^{-2})	surface tension[b] (mN m^{-1})	capillary length (L_c) (mm)	evaporative flux (g h^{-1} cm^{-2})	normalization constant
MeOH	0.406	0.763	20.21	1.64	0.043	1.89
EtOH	0.673	0.763	19.82	1.62	0.023	1.00
i-PrOH	1.052	0.759	18.69	1.58	0.018	0.76
t-BuOH	1.428	0.754	17.70	1.56	0.021	0.88

[a]Literature values from refs 9−11. [b]Literature values from refs 14, 15.
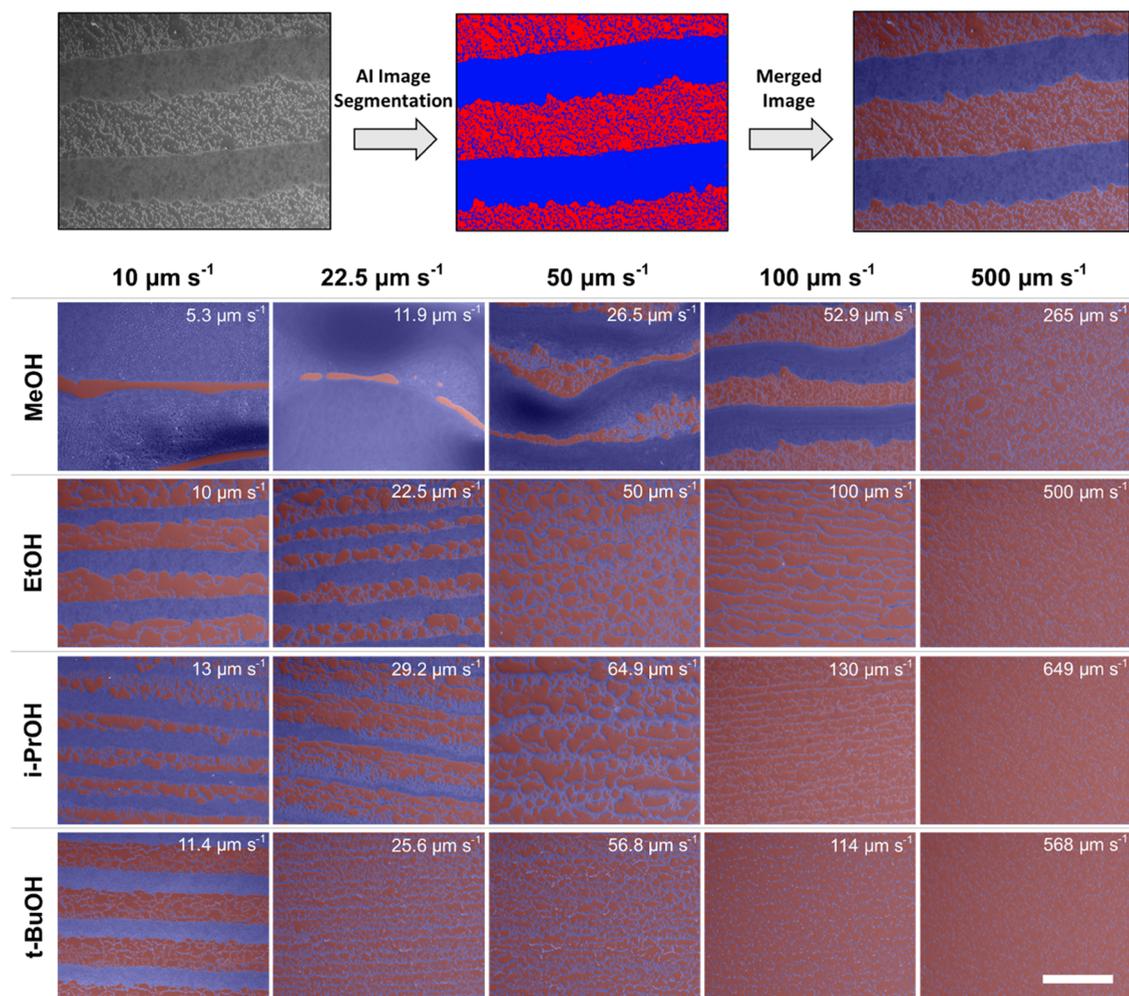

Figure 1. Colloidal films prepared via dip-coating in different solvents at different withdrawal rates using 0.1 vol % 250 nm SiO$_2$ particles with a chamber temperature of 50 °C. Images were segmented to allow quantification of surface coverage and colored to improve the contrast between regions of particles (blue) and substrate (red). Each image has been annotated with withdrawal velocities corrected to account for variations in the evaporation rate (white text, see Section S5 for details). All images were taken at the same magnification. Scale bar = 50 μm.

inhomogeneous and poorly reproducible depositions. High temperatures can also lead to the Bénard−Marangoni effect, where the surface tension varies due to a temperature gradient across the meniscus, leading to circular currents within the meniscus.[5] One parameter that is conspicuously absent from the evaporative transport equation, and thus never independently examined, is solvent viscosity. But, is it true that viscosity has zero impact on particle transport? And how does viscosity impact particle distribution on the substrate?

Cui et al. have proposed that higher viscosity increases the resistance to outward particle flow, but many physical parameters were simultaneously changed, including contact angle, surface tension, and evaporation rate.[3] Noguera-Marín et al. proposed a relationship between collective diffusion

during convective assembly and viscosity.[6] An increased viscosity has also been attributed to delaying meniscus displacement.[7,8]

In this article, for the first time, we study the effect of viscosity on evaporative flux as an isolated parameter. Silica particles are used as model systems, both spherical and in the form of nanoribbons, assembled using dip-coating. We investigate particle assembly in both single and binary dispersant phases and show that surface tension gradients formed during evaporation in the binary system heavily impact assembly patterns. Finally, we show how evaporative flux in a binary solvent system leads to differences in self-assembly patterns. Control over particle patterning is of interest as
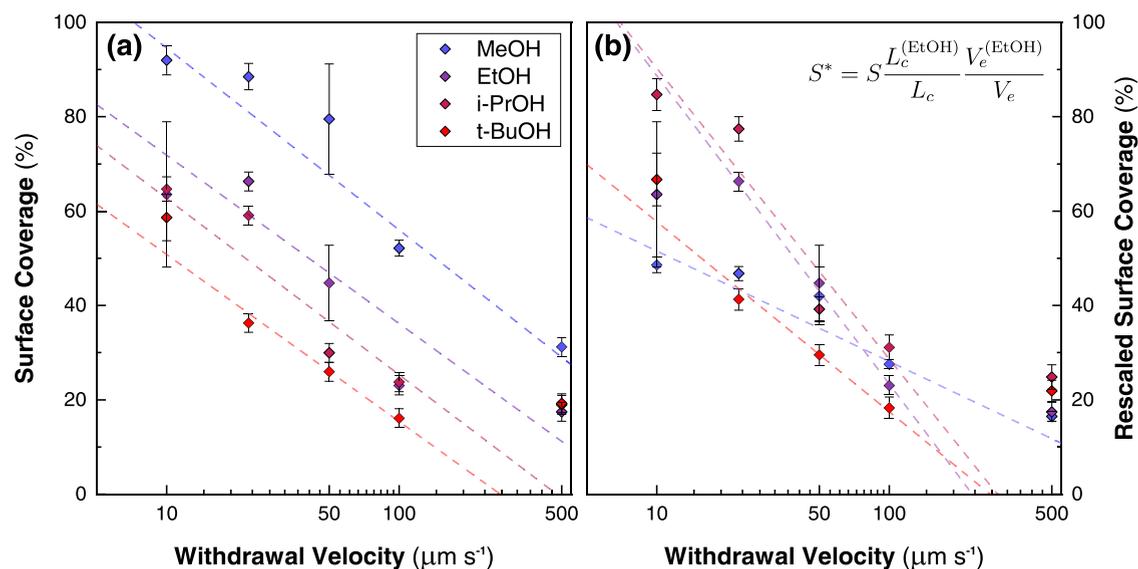
Figure 2. (a) Surface coverage as a function of withdrawal velocity for different solvents. Coverage was calculated from the segmentation of multiple images at 1.15×10^4 μm. (b) Surface coverage rescaled according to the inset equation.

scaffolds for biological media, for optically active substrates, and as masks for substrate processing.

RESULTS AND DISCUSSION

To determine if there is an effect of solvent viscosity on convective particle depositions, four alcohols with different viscosities were selected: methanol (MeOH), ethanol (EtOH), isopropanol (i-PrOH), and *tert*-butanol (t-BuOH). Each time an additional carbon atom is added to the alcohol molecule in this series of solvents, the viscosity at 50 °C increases by a factor of ~1.5 (Table 1).[9−11] Other physical properties of these alcohols, like density, surface tension, capillary length, and evaporative flux, are quite similar (Figure S1). Table 1 lists these physical properties at 50 °C, a temperature chosen because it was the chamber temperature during evaporation-induced particle self-assembly. The densities of the solvents are very close to one another, which means that the buoyancy of the particles will be roughly equivalent. The surface tensions, which dictate contact angle and capillary length, are also similar for this series of alcohols. Thus, the calculated capillary lengths, which are the typical length over which the evaporation contributes to particle deposition in a film, are also comparable for these solvents. The substrate is highly wetted by all four solvents, making it impossible to measure the contact angle. However, convective flow can bring particles to the drying line even when the contact angle is below 15°.[12] Evaporative flux relates to how fast the solvent molecules diffuse away from the liquid−air contact line upon evaporation.[13] The evaporation rate increases with increasing solvent vapor diffusion away from this interface leading to higher convective flux toward the meniscus. Although a strong correlation between evaporative flux and carbon chain length has been observed in the past,[13] we measure similar values for EtOH, i-PrOH, and t-BuOH (Figure S1d) at 50 °C, which we attribute to the branching of the longer chain alcohols that seems to increase their evaporative flux. MeOH was found to have an evaporative flux approximately double that of the other solvents, attributed to its higher volatility. Among these solvents, there are small variations in solvent properties with a large variation in viscosity. Thus, if viscosity were to have an

effect, we expect to observe it beyond the contribution of the other multiple factors.

For the self-assembly studies, silica spherical particles were produced using a seeded Stöber synthesis (Figure S2), which had a mean diameter of (250 ± 3) nm (Figure S3). The monodispersity of these particles is helpful in obtaining close-packed, organized assemblies.[16] The particles were then deposited onto silicon wafers via dip-coating in a temperature-controlled chamber. Figure 1 shows SEM images of films prepared in MeOH, EtOH, i-PrOH, and t-BuOH over a range of speeds within the convective and the transitional convective/advective regime, with higher magnification images shown in Figure S4. The images have been treated so that the sections of bare substrate appear red, and the areas with particle coverage are displayed in blue. Stick-slip behavior is observed for all solvents, due to meniscus pinning at low withdrawal speeds. However, stick-slip banding is not equivalent for all solvents: stick-slip only becomes prominent at very low speeds for higher viscosity solvents. To distinguish the effect of viscosity from those due to differences in the evaporative flux, the velocities were normalized relative to the rate of evaporation of EtOH (Figure 1 and Section S5). No obvious correlation can be seen between the corrected velocity values and the observed particle patterning, supporting the conclusion that the change in stick-slip patterning results from viscosity. The most homogeneous films were produced for t-BuOH, having the highest viscosity. As viscosity is the resistance to motion in a fluid, intuitively, viscous forces should impact the depinning of the meniscus. It does appear to impact the particle patterning. Particle distribution should not be confused with total surface coverage, which can be studied quantitatively.

The particle coverage was investigated for these films, as a function of speed and solvent. The observed increase in particle coverage with decreasing substrate withdrawal speeds is expected in the evaporative regime.[1,17] The higher volatility of MeOH, compared with the other solvents, produced films that were much thicker at lower withdrawal speeds; these were often disordered multilayer films with variable thicknesses and gaps. When MeOH was used as the dispersant phase, all of the
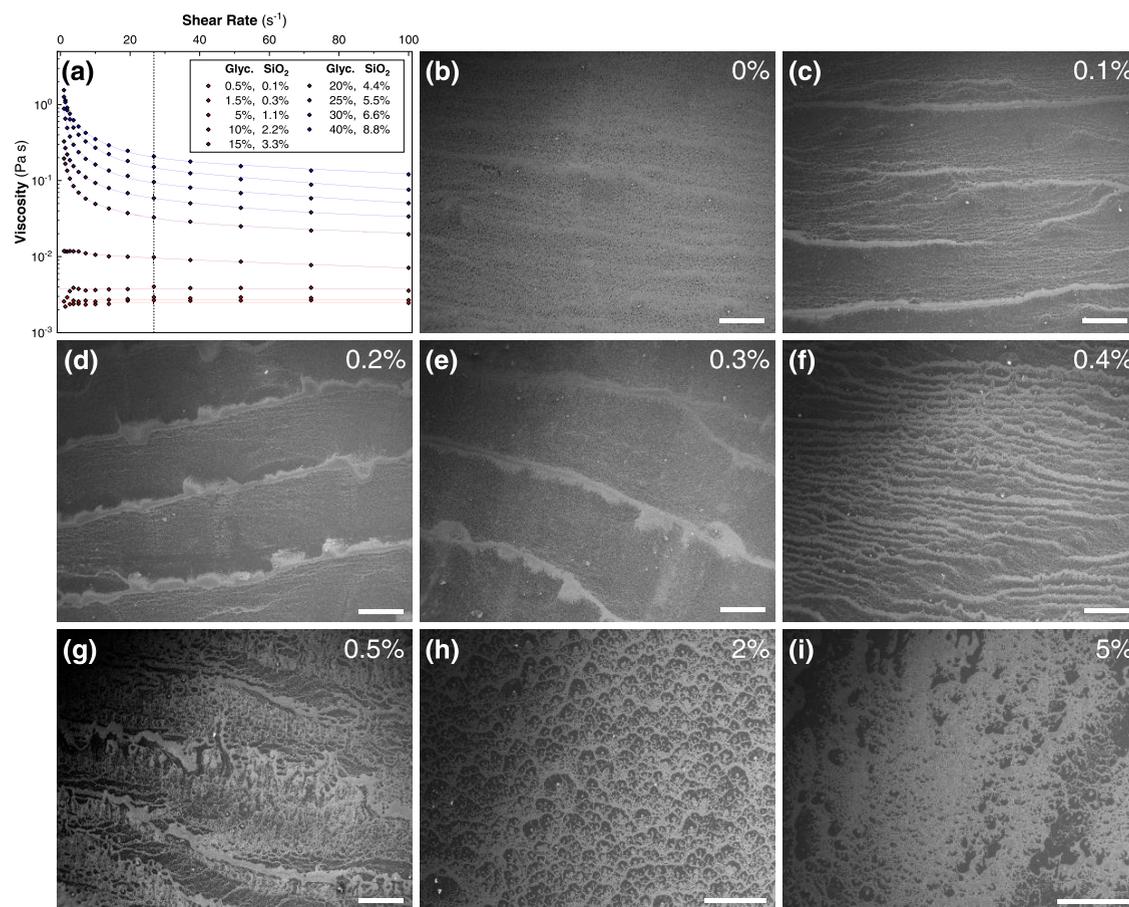
Figure 3. (a) Dynamic viscosity of i-PrOH−glycerol−SiO$_2$ particle mixtures as a function of shear rate. SEM images of dip-coated films prepared at 50 °C, withdrawn at 50 μm s^{-1}, using an initial concentration of 0.11 vol % SiO$_2$ particles and (b) 0 vol %, (c) 0.1 vol %, (d) 0.2 vol %, (e) 0.3 vol %, (f) 0.4 vol %, (g) 0.5 vol %, (h) 2 vol %, and (i) 5 vol % glycerol. Dark gray zones represent bare substrates, and light gray regions contain particles. The scale bar represents 60 μm for all images.

observed banded stick-slip structures at lower speeds were multilayer. All other films, for all of the other solvents, consisted of a single layer of particles of varying coverage fraction.

Particle surface coverage was calculated through the segmentation of six images containing areas of 1.15×10^4 μm^2 from two replicate samples for each condition. The surface coverage was then expressed as the percentage of pixels identified as particles (Figure 2). Decreasing surface coverage can be seen with solvent viscosity (Figure 2a). However, before concluding that viscosity impacts surface coverage, it is worth normalizing for the minor changes in other physical properties using the normalization constants given in Table 1, which are explained further in Section S5. Equation S4 gives the expected surface coverage when rescaled by the capillary length and evaporation rate of EtOH. Any difference in the relative magnitudes of the surface coverage before and after rescaling suggests that evaporative effects are responsible for the observed changes in surface coverage. The rescaled values are plotted in Figure 2b, demonstrating that not only do the observed surface coverages change relative to each other, but there is no longer a clear trend between viscosity and surface coverage. This suggests that any effect of viscosity on surface coverage is insignificant relative to the effect of the differences in evaporative flux, quantified by eq 1.

Viscosity seems to impact the patterning, but not surface coverage. The most common way of changing the viscosity is

to use a two-solvent system. Doing so is problematic for several reasons. The first is that by adding a second solvent, usually a highly viscous polymer or molecule, the surface tension may change in addition to viscosity. Moreover, the volatility of the two co-solvents is typically not the same, leading to an enrichment of one solvent during the drying process. Thus, a gradient in solvent composition establishes, leading to a gradient in viscosity and surface tension, generating highly complicated Marangoni flow patterns. In some cases, a gradient in evaporative flux is generated as well, if the two solvents have different evaporation rates.

We studied the combination of glycerol and i-PrOH to vary viscosity. In this co-solvent system, only i-PrOH is volatile at 50 °C, meaning that glycerol will stay embedded between SiO$_2$ particles. The changing volume fractions of the three components, i-PrOH, glycerol, and silica, are shown as a function of evaporated i-PrOH in Figure S5 and Table S1. We observe that viscosities vary linearly with glycerol concentration between the values of pure i-PrOH (2.86 mPa s) and glycerol (1.47 Pa s) (Figure S6).[18] However, the viscosity of the particle solutions also depends on particle concentration. When the viscosity is measured with a relative enrichment in both glycerol and silica particles, we see that the viscosity increases more significantly than for glycerol alone (Figures 3 and S7). The surface tension of i-PrOH/glycerol solutions has been reported in the literature, showing that surface tension stays roughly constant up to ~70% glycerol content and then
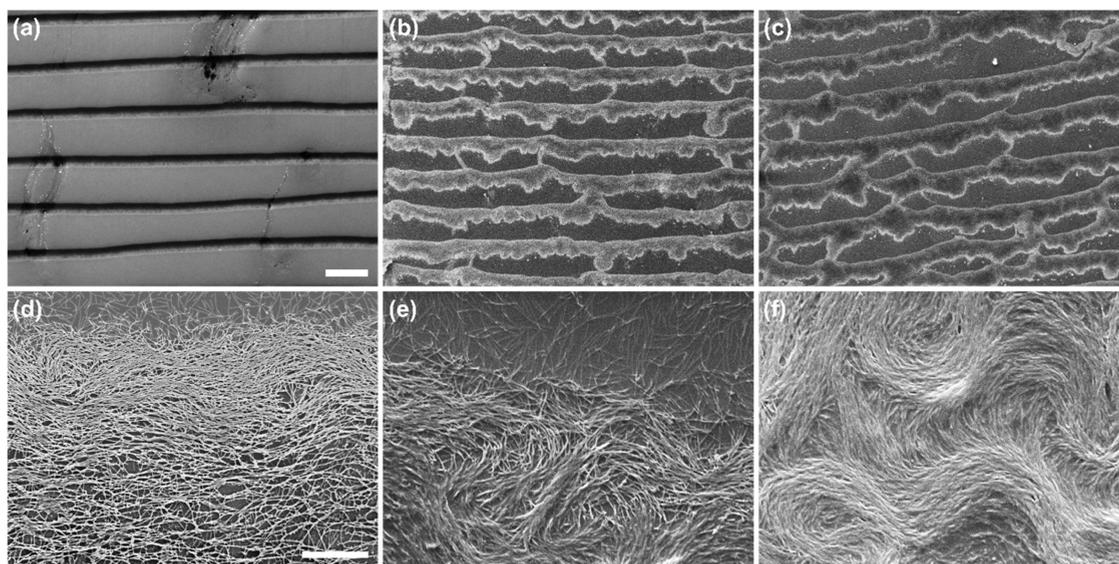
Figure 4. Temperature effect on the pattern of the anisotropic particle deposition. SEM images of ribbons deposited on silicon substrates when the chamber temperature is (a, d) 25 °C, (b, e) 35 °C, and (c, f) 55 °C, at (a−c) low and (d−f) high magnification. The SiO$_2$/poly(acrylic acid) ratio is 1:10, the silica concentration is 0.4 mg mL^{-1}, and the withdrawal speed is 10 μm s^{-1}. Dark gray zones represent bare substrates, and light gray regions contain particles. Scaling is the same for (a−c) and (d−f). Scale bar in (a) = 200 μm and in (c) = 2 μm.

ramps up very rapidly to high values (Figure S8).[19] The surface tension of glycerol is three times higher than that of pure i-PrOH. Thus, there will be a significant gradient in surface tension across the meniscus due to i-PrOH evaporation. The evaporation rate is initially constant, decreasing linearly while enriching the system in glycerol, and then decreases as the system becomes significantly enriched in glycerol (Figure S9). Thus, there is a gradient in surface tension, viscosity, and evaporative flux during the drying process.

We found that at very low glycerol content (0.1−0.3 vol %), there was a very large impact on the stick-slip behavior (Figures 3 and S10). In opposition to the single-solvent viscosity study, an increase in viscosity provoked more marked stick-slip banding, with more interband particle deposition. Break-up happens for a large-enough Marangoni number, a dimensionless parameter comparing the relative effects of surface tension and viscous forces. Thus, both surface tension and viscous forces will impact pinning and interband distance. In the case of the single solvents, increasing viscosity decreased the propensity for pinning, leading to a more homogeneous coverage. In the co-solvent case, the viscosity increases much faster than the surface tension in the initial moments of pinning. But, the Marangoni number will increase rapidly as the alcohol evaporates, encouraging break-up. By 0.4 vol % glycerol content, the distance between banding dropped dramatically as pinning and depinning became more frequent and more erratic. This behavior is consistent with Marangoni flows away from the contact line. By 0.5 vol % glycerol, the film pattern was completely disordered. Increasing to 2 vol %, glycerol content generated lacy patterns, as if beading were occurring. By 5 vol %, a mixture of mono- and multilayer regions is observed on a highly inhomogeneous surface. What is certain is that the quantity of particle deposition increases with increasing glycerol content, but at the expense of reproducibility, homogeneity, and an understanding of the deposition process. We find it impossible to tease out the contributions of surface tension and viscosity gradients across the meniscus in the co-solvent system.

To better understand the stick-slip banding in a co-solvent system (poly(acrylic acid) in i-PrOH), anisotropic silica particles, in the form of long ribbons (0.5−1.0 μm in length, ∼20 nm in width), were studied. The ribbons are semi-flexible and thus can follow the flow pattern of the Marangoni currents, providing evidence for the currents upon drying. Based on our previous study,[1] the ribbons dispersed in poly(acrylic acid)/i-PrOH were deposited at three different temperatures to investigate the flow instabilities as a function of drying speed (Figure 4). At room temperature, no evidence for flow instabilities was detected, and the ribbons were aligned parallel to the meniscus and largely parallel to each other. Thus, it seems that break-up occurs before a significant gradient in surface tension establishes at ambient temperature. Both the leading and trailing edge were clean, attesting to classical stick-slip behavior. As the temperature in the chamber was increased to 35 and 55 °C, the leading edge remained clean and the trailing edge showed swirling patterns. The organization of the ribbons parallel to the swirling patterns reveals the direction of the Marangoni flow current. Pinning seems to occur regularly, creating a linear band at the leading edge. As in the co-solvent system for the spherical silica particles, a gradient in surface tension must be created before break-up, due to the evaporation of the alcohol. Marangoni flows in a sessile droplet, in the presence of 0.5 wt % PEG, have been studied by Seo et al., where they observed a delay of 10 s before a surface tension gradient generated, and the Marangoni flow began.[20] Perhaps before break-up, as surface tension begins to increase at the trailing edge, a flow instability is created where the silica particles try to flow away from the drying line, rather than in the direction of convective flux. The co-solvent system clearly has several competing forces that make studying these systems rather complex.

■ CONCLUSIONS

We have studied the impact of solvent viscosity, surface tension, and evaporation rate on particle patterning and surface coverage in films deposited via evaporation-induced self-

assembly using dip-coating. Both single-solvent and co-solvent systems were studied. While viscosity did not affect surface coverage, it had a visible impact on particle arrangement. Surface coverage was sensitive to changes in evaporative flux. The single and co-solvent systems did not give the same results regarding patterning: in the single-solvent system, viscosity decreased the propensity for banding arising from the stick-slip phenomenon, whereas in the co-solvent system, marked banding occurred despite an increase in viscosity. This difference in banding distance depends on both viscosity and surface tension, where surface tension appears to have a greater influence.

Gradients in surface tension rely on fast evaporation. When the chamber temperature was increased, a more significant surface tension gradient was established, generating Marangoni flow patterns. These could be visualized post-synthetically from the deposition patterns of semi-flexible ribbons.

In pursuit of homogeneous monolayer films, it seems there are two important factors: (1) to avoid generating gradients by using a single-solvent system and (2) to suppress depinning events by increasing the ratio between viscosity and surface tension forces.

■ METHODS

Materials. Isopropanol (i-PrOH, ≥99.5%, 190764), glycerol (≥99.5%, G7893), tetraethyl orthosilicate (≥99.0%, 86578), ammonium hydroxide solution (29%, 221228), L-arginine (≥99.5%, 11009), methanol (MeOH, ≥99.8%, 322415), and *tert*-butanol (*t*-BuOH, ≥99%, 360538) were purchased from Sigma-Aldrich. Ethanol (EtOH, 99.9%, PC80101.9200) was supplied by Atlantic Labo. All chemicals were used without further purification. Aqueous solutions were prepared using deionized water, prepared using a Type 1 Milli-Q water purification system (18.2 MΩ cm).

Characterization. Particles were imaged using a JEOL 1400F TEM using a 120 kV acceleration voltage. Dip-coated particle films were imaged using a JEOL JSM 6700F SEM using a 10 kV acceleration voltage using a SEI detector at a working distance of 6 mm. Images of films were then segmented using the Trainable Weka Segmentation ImageJ plugin.[21] Viscosities were measured using a TA Instruments AR2000 rheometer equipped with a 60 mm cone plan geometry.

30 nm SiO_2 Nanoparticle Seed Synthesis. Following a protocol first published by Hartlen et al.[22] and optimized by Désert et al.[23,24] 6 mM aqueous L-arginine (100 mL) was added to a 150 mL single-necked, flat-bottomed cylindrical jacketed reaction vessel (internal diameter ~4 cm). The solution was put under stirring (150 rpm, 30 × 8 mm² Teflon-coated stir bar) under reflux. To this was then added 10 mL tetraethyl orthosilicate which remained in a separate phase to the aqueous solution. The mixture was left until the upper tetraethyl orthosilicate phase completely vanished (~2 days). A small volume of the seed solution was checked by TEM before use and confirmed to be (30 ± 3) nm (Figure S2). The concentration of the sample was determined by dry extraction to be ~14.5 g L^{-1} (~4.7 × 10^{14} mL^{-1}).

Regrowth of SiO_2 Particles to 250 nm. The 30 nm silica seed particles were regrown to a larger size following a seeded Stöber approach. EtOH (910 mL) and ammonium hydroxide solution (70 mL) were mixed in a 2 L round-bottomed flask to which 1.6 mL of the 30 nm SiO_2 nanoparticle suspension was added under stirring. Tetraethyl orthosilicate (100 mL) was then added by a syringe pump (KD Scientific, 78-9100F) at a rate of 1.4 mL h^{-1} through a cannula (Braun, Venofix A). The solution was left for ~24 h after the tetraethyl orthosilicate addition had been completed. The ammonia was removed, and the volume of the nanoparticle solution was reduced by rotary evaporation (ice-cooled condenser, 60 °C, 0.2 atm, 240 rpm). Once a suitable volume had been reached, the particles were cleaned by centrifugation (3000g, 5 min) before resuspension in

a fresh solvent (MeOH, EtOH, i-PrOH, or *t*-BuOH). The size of the particles was determined to be (250 ± 3) nm by TEM (Figure S3). The concentration of the particles was determined by dry extraction to be 26.9 g L^{-1} (1.5 × 10^{12} mL^{-1}).

Silica Ribbon Colloidal Solutions. The silica ribbon suspensions were prepared following three steps: synthesis of the organic template, silica transcription, and ribbon dispersion; each of which has been described by Okazaki et al.[25]

Step 1: the synthesis of organic surfactant template C_2H_4-*1,2*-$((CH_3)_2N^+C_{16}H_{33})_2$ with a tartrate counterion, also named 16-2-16 Gemini L-tartrate, was optimized in a previous work.[25] First, 16-2-16 Gemini bromide was obtained from the reaction of *N,N,N′,N′*-tetramethylethylenediamine with 1-bromohexadecane. Then, silver acetate was used to replace the bromide in 16-2-16 Gemini bromide, giving the product 16-2-16 Gemini acetate. Finally, L-tartrate was chosen for the ion exchange of the acetate to give the 16-2-16 Gemini L-tartrate. The complex self-assembled in water to form twisted ribbons. A 1 mM 16-2-16 L-tartrate aqueous solution was heated to 60 °C for 15 min, and then the solution was cooled to 20 °C for 2 h.

Step 2: Tetraethyl orthosilicate (500 μL) was added to 10 mL of 0.1 mM aqueous solution of L-tartaric acid (pH 3.8) and prehydrolyzed at 20 °C by stirring on a roller-mixer for 7 h. Then, equal volumes of prehydrolyzed tetraethyl orthosilicate and organic gels containing the ribbons were mixed (typically, 4 mL of each) and stirred at 20 °C with a roller-mixer overnight. The excess silica precursor and organic template were washed away by i-PrOH using a centrifuge.

Step 3: A high-intensity ultrasonic processor (Vibra cell 75186) equipped with a 2 mm microtip with variable power was used (maximum power, 130 W). A 20 kHz pulse mode was used for the dispersion and fragmentation of silica ribbons. Silica ribbons (2 mg) were mixed with 2 mL of i-PrOH and sonicated for 15 min with pulses of 1 s, separated by 1 s pauses. Samples were cooled in an ice bath during the sonication process to avoid solvent evaporation and an increase in the sample temperature, which could influence the fragmentation process.

Step 4: Poly(acrylic acid) was dissolved in i-PrOH to a concentration of 20 g L^{-1}. The polymer solutions and silica suspensions were mixed and then sonicated for 10 min in an ultrasound bath to produce homogeneous suspensions.

Dip-Coating. Dip-coating experiments were performed on a SolGelWay ACEdip 2.0 dip-coater. The withdrawal speed and chamber temperature were controlled via a computer. Boron-doped prime CZ silicon wafers with (100) orientation were obtained from Sil′tronix. The wafers were stored in 3 M nitric acid until they were required for use, after which they were rinsed with water, and excess liquid was removed using compressed air. The substrates were then treated using an ozone cleaner (Novascan, PSD Proseries & OES-1000D) for 10 min before being placed in the dip-coating chamber.

Evaporation Studies. Each solvent (100 g) was placed inside an oven at 50 °C in an 8 cm diameter beaker, and the mass of the beaker was recorded periodically until all solvent was evaporated. The evaporation rate was then determined from a linear fit to the mass loss over time.

■ ASSOCIATED CONTENT

Data Availability Statement

All data associated with this manuscript is available free of charge from https://www.doi.org/10.5281/zenodo.7248994.

ⓢ Supporting Information

The Supporting Information is available free of charge at https://pubs.acs.org/doi/10.1021/acs.langmuir.2c02890.

> Physical properties of methanol, ethanol, isopropanol, and *tert*-butanol; characterization of silica seed particles and 250 nm silica particles; higher magnification SEM micrographs of deposited films; methodology for normalization of withdrawal velocities and surface coverage; isopropanol/glycerol/silica composition evo-

lution during evaporation; rheology of isopropanol−glycerol and isopropanol−glycerol-silica mixtures; tensiometry of isopropanol−glycerol mixtures (PDF)

■ AUTHOR INFORMATION

Corresponding Authors

Lucien Roach − *Université de Bordeaux, CNRS, Bordeaux INP, ICMCB, UMR 5026, F-33600 Pessac, France;* ● orcid.org/0000-0002-9166-6662; Email: lucien.roach@icmcb.cnrs.fr

Glenna L. Drisko − *Université de Bordeaux, CNRS, Bordeaux INP, ICMCB, UMR 5026, F-33600 Pessac, France;* ● orcid.org/0000-0001-6469-9736; Email: glenna.drisko@icmcb.cnrs.fr

Authors

David Gonzalez-Rodriguez − *Université de Lorraine, LCP-A2MC, 57000 Metz, France*

Jie Gao − *Université de Bordeaux, CNRS, Bordeaux INP, CBMN, UMR 5248, F-33600 Pessac, France*

Eric Laurichesse − *Université de Bordeaux, CNRS, CRPP, UMR 5031, 33600 Pessac, France*

Alexander Castro-Grijalba − *Université de Bordeaux, CNRS, Bordeaux INP, ICMCB, UMR 5026, F-33600 Pessac, France*

Reiko Oda − *Université de Bordeaux, CNRS, Bordeaux INP, CBMN, UMR 5248, F-33600 Pessac, France; WPI-Advanced Institute for Materials Research, Tohoku University, 980-8577 Sendai, Japan;* ● orcid.org/0000-0003-3273-8635

Véronique Schmitt − *Université de Bordeaux, CNRS, CRPP, UMR 5031, 33600 Pessac, France*

Emilie Pouget − *Université de Bordeaux, CNRS, Bordeaux INP, CBMN, UMR 5248, F-33600 Pessac, France;* ● orcid.org/0000-0002-3175-6201

Mona Tréguer-Delapierre − *Université de Bordeaux, CNRS, Bordeaux INP, ICMCB, UMR 5026, F-33600 Pessac, France;* ● orcid.org/0000-0002-3096-6645

Complete contact information is available at:
https://pubs.acs.org/10.1021/acs.langmuir.2c02890

Author Contributions

L.R., D.G.-R., and G.L.D. were involved in the writing of the original draft and visualization. L.R. and D.G.-R. contributed to the methodology and formal analysis. L.R., J.G., A.C.-G., and E.L. were responsible for the investigation. M.T.-D., R.O., E.P., V.S., and G.L.D. were involved in supervision and procuring resources. G.L.D. was responsible for project administration and funding acquisition. All authors were involved in the reviewing and editing of the final manuscript. All authors have given approval to the final version of the manuscript.

Notes

The authors declare no competing financial interest.

■ ABBREVIATIONS

MeOH, methanol; EtOH, ethanol; i-PrOH, isopropanol; *t*-BuOH, *tert*-butanol; SEM, scanning electron microscopy; TEM, transition electron microscopy

■ REFERENCES

(1) Gao, J.; Semlali, S.; Hunel, J.; Montero, D.; Battie, Y.; Gonzalez-Rodriguez, D.; Oda, R.; Drisko, G. L.; Pouget, E. Creating Regular Matrices of Aligned Silica Nanohelices: Theory and Realization. *Chem. Mater.* 2020, 32, 821.

(2) Shen, X.; Ho, C.-M.; Wong, T.-S. Minimal Size of Coffee Ring Structure. *J. Phys. Chem. B* 2010, 114, 5269.

(3) Cui, L.; Zhang, J.; Zhang, X.; Huang, L.; Wang, Z.; Li, Y.; Gao, H.; Zhu, S.; Wang, T.; Yang, B. Suppression of the Coffee Ring Effect by Hydrosoluble Polymer Additives. *ACS Appl. Mater. Interfaces* 2012, 4, 2775.

(4) Han, W.; Lin, Z. Learning from "Coffee Rings": Ordered Structures Enabled by Controlled Evaporative Self-Assembly. *Angew. Chem., Int. Ed.* 2012, 51, 1534.

(5) Karbalaei, A.; Kumar, R.; Cho, H. J. Thermocapillarity in Microfluidics-A Review. *Micromachines* 2016, 7, 13.

(6) Noguera-Marín, D.; Moraila-Martínez, C. L.; Cabrerizo-Vílchez, M.; Rodríguez-Valverde, M. A. Impact of the Collective Diffusion of Charged Nanoparticles in the Convective/Capillary Deposition Directed by Receding Contact Lines. *Eur. Phys. J. E* 2016, 39, 20.

(7) Luo, H.; Gersappe, D. Dewetting Dynamics of Nanofilled Polymer Thin Films. *Macromolecules* 2004, 37, 5792.

(8) Hong, S. W.; Xia, J.; Byun, M.; Zou, Q.; Lin, Z. Mesoscale Patterns Formed by Evaporation of a Polymer Solution in the Proximity of a Sphere on a Smooth Substrate: Molecular Weight and Curvature Effects. *Macromolecules* 2007, 40, 2831.

(9) Gong, Y.-H.; Shen, C.; Lu, Y.-Z.; Meng, H.; Li, C.-X. Viscosity and Density Measurements for Six Binary Mixtures of Water (Methanol or Ethanol) with an Ionic Liquid ([BMIM][DMP] or [EMIM][DMP]) at Atmospheric Pressure in the Temperature Range of (293.15 to 333.15) K. *J. Chem. Eng. Data* 2012, 57, 33.

(10) Bravo-Sánchez, M. G.; Iglesias-Silva, G. A.; Estrada-Baltazar, A.; Hall, K. R. Densities and Viscosities of Binary Mixtures of N-Butanol with 2-Butanol, Isobutanol, and Tert-Butanol from (303.15 to 343.15) K. *J. Chem. Eng. Data* 2010, 55, 2310.

(11) Shirazi, S. G.; Kermanpour, F. Density and Viscosity of 2-Butanol + (1-Propanol, 2-Propanol, or 3-Amino-1-Propanol) Mixtures at Temperatures of (293.15 to 323.15) K: Application of the ERAS Model. *J. Chem. Eng. Data* 2019, 64, 2292.

(12) Malaquin, L.; Kraus, T.; Schmid, H.; Delamarche, E.; Wolf, H. Controlled Particle Placement through Convective and Capillary Assembly. *Langmuir* 2007, 23, 11513.

(13) Carle, F.; Semenov, S.; Medale, M.; Brutin, D. Contribution of Convective Transport to Evaporation of Sessile Droplets: Empirical Model. *Int. J. Therm. Sci.* 2016, 101, 35.

(14) Bagheri, A.; Moradian, Z. Equilibrium Surface Tension and the Interaction Energy of DMSO with Tert-Butyl Alcohol or Iso-Amyl Alcohol at Various Temperatures. *J. Chem. Thermodyn.* 2014, 78, 16.

(15) Vazquez, G.; Alvarez, E.; Navaza, J. M. Surface Tension of Alcohol Water + Water from 20 to 50 °C. *J. Chem. Eng. Data* 1995, 40, 611.

(16) Lacks, D. J.; Wienhoff, J. R. Disappearances of Energy Minima and Loss of Order in Polydisperse Colloidal Systems. *J. Chem. Phys.* 1999, 111, 398.

(17) Faustini, M.; Louis, B.; Albouy, P. A.; Kuemmel, M.; Grosso, D. Preparation of Sol—Gel Films by Dip-Coating in Extreme Conditions. *J. Phys. Chem. C* **2010**, *114*, 7637.

(18) Yu, M.; Qiao, X.; Dong, X.; Sun, K. Shear thickening effect of the suspensions of silica nanoparticles in PEG with different particle size, concentration, and shear. *Colloid Polym. Sci.* **2018**, *296*, 1119—1126.

(19) Erfani, A.; Khosharay, S.; Aichele, C. P. Surface Tension and Interfacial Compositions of Binary Glycerol/Alcohol Mixtures. *J. Chem. Thermodyn.* **2019**, *135*, 241.

(20) Seo, C.; Jang, D.; Chae, J.; Shin, S. Altering the Coffee-Ring Effect by Adding a Surfactant-like Viscous Polymer Solution. *Sci. Rep.* **2017**, *7*, No. 500.

(21) Arganda-Carreras, I.; Kaynig, V.; Rueden, C.; Eliceiri, K. W.; Schindelin, J.; Cardona, A.; Sebastian Seung, H. Trainable Weka Segmentation: A Machine Learning Tool for Microscopy Pixel Classification. *Bioinformatics* **2017**, *33*, 2424.

(22) Hartlen, K. D.; Athanasopoulos, A. P. T.; Kitaev, V. Facile Preparation of Highly Monodisperse Small Silica Spheres (15 to >200 nm) Suitable for Colloidal Templating and Formation of Ordered Arrays. *Langmuir* **2008**, *24*, 1714.

(23) Désert, A.; Chaduc, I.; Fouilloux, S.; Taveau, J.-C.; Lambert, O.; Lansalot, M.; Bourgeat-Lami, E.; Thill, A.; Spalla, O.; Ravaine, S.; Duguet, E. High-Yield Preparation of Polystyrene/Silica Clusters of Controlled Morphology. *Polym. Chem.* **2012**, *3*, 1130.

(24) Désert, A. Colloides Hybrides Silice/Polystyrène de Morphologie Contrôlée, PhD Thesis, Université de Bordeaux, 2011.

(25) Okazaki, Y.; Cheng, J.; Dedovets, D.; Kemper, G.; Delville, M.-H.; Durrieu, M.-C.; Ihara, H.; Takafuji, M.; Pouget, E.; Oda, R. Chiral Colloids: Homogeneous Suspension of Individualized SiO_2 Helical and Twisted Nanoribbons. *ACS Nano* **2014**, *8*, 6863.